Francke, H., Thorade, M. (2010): Density and viscosity of brine: An overview from a process engineers perspective. - Chemie der Erde - Geochemistry, 70, Suppl. 3, 23-32

DOI: 10.1016/j.chemer.2010.05.015

Density and viscosity of brine: an overview from a process engineers perspective

Henning Francke[a], Matthis Thorade[a]

[a]*Helmholtz Centre Potsdam, GFZ German Research Centre for Geosciences, Telegrafenberg, 14437 Potsdam, Germany*

Abstract

The aim of our study is to evaluate the sensitivity of the volumetric flow rate of a downhole pump in a geothermal production well on different density and viscosity functions during the startup and stationary operating phases. The geothermal fluid is modeled as an aqueous sodium chloride solution and functions for its density and viscosity are compared and applied to a model of the geothermal fluid cycle. It is shown that the deviations between viscosity functions have negligible impact on the the volumetric flow rate, while the impact of the deviations between different density functions is up to 54 % of the volumetric flow rate.

Keywords: density, viscosity, brine, aqueous sodium chloride solution, geothermal energy, pressure profile, pumping requirements

1. Introduction

Geothermal heat and power plants use hot geothermal fluid as a transport medium to extract thermal energy from the deep underground. A downhole pump in the production well lifts the brine up to the surface, where it is cooled in a heat exchanger and reinjected subsequently (Fig. 1). As the downhole pump consumes a significant quantity of energy, special attention should be paid to its dimensioning (Saadat et al., 2008). For this task, knowledge of thermophysical and transport properties of the brine are indispensable. These properties are determined by pressure, temperature and chemical composition.

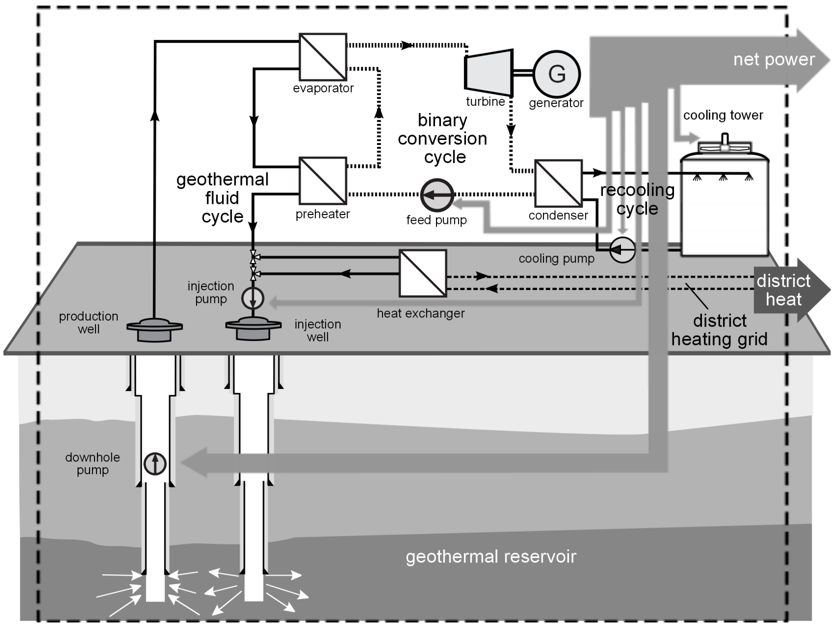

Figure 1: Schematic diagram of an exemplary geothermal fluid cycle. Exemplarily a power plant and district heating station are shown as thermal energy consumers. The downhole pump consumes a significant quantity of energy.

Functions for the calculation of property values are usually mathematical expressions fitted to reproduce experimentally measured values. Adams and Bachu (2002) reviewed various functions for the calculation of brine density and viscosity.

Champel (2006) used different density functions to calculate the density change resulting from the temperature change of the fluid inside the wells after initiation of fluid extraction.

Two important aspects of pump dimensioning consist of the calculation of the volumetric flowrate and the power needed to produce this flowrate. During the planning period of a geothermal site exact fluid properties are usually not available. The aim of our study is to evaluate the sensitivity of the volumetric flow rate on different density and viscosity functions during the startup and stationary operation of a sample power plant. The boundary conditions assumed are similar to those found in our test site in Groß Schönebeck, 50 km north of Berlin, constituting a representative example for a geothermal system in the North German Basin (Zimmermann et al., 2009).

2. Methodological approach

The general approach of this study is to apply different property functions from literature to a model of the geothermal fluid cycle and evaluate the resulting impact on the volumetric flow rate.

2.1. Geothermal fluid property functions

Geothermal fluids with salinities higher than 10 g/l are generally Cl-dominated, with Cl accounting for over 95 % by mass of anions. In low to moderate salinity fluids, Na is the dominant cation. As brine salinity increases, the relative proportion of Na decreases and the proportions of K, Mg and Ca increase. Most noteable is the increase in Ca, which typically is the dominant cation by mass in fluids whose salinities exceed 300 g/l (Hanor, 1994).

Given the dominance of Cl and Na ions over a wide range of salinity relevant for geothermal fluids, these fluids are frequently modeled as aqueous NaCl solutions (Adams and Bachu, 2002). The total of dissolved solids in the fluid found in Groß Schönebeck sums up to 265 g/l (Huenges and Winter, 2004). We modeled the fluid as an aqueous sodium chloride solution with a NaCl mass fraction of 0.225 $kg_{NaCl}/kg_{Solution}$, corresponding to a molality of 4.968 mol_{NaCl}/kg_{H_2O}. For the conversion between mass fraction w, mole fraction x and molality b see Appendix A.

2.1.1. *Density*

An overview on the density functions used is given in Table 1.

Table 1: Applicability range of various algorithms for calculating brine density.

Study	T / °C	p / MPa	Electrolytes	b / $mol \cdot kg^{-1}$
Rowe and Chou (1970)*	20 - 150	p_{sat} - 35	NaCl	0 - 5.7
Phillips et al. (1981)	10 - 350	p_{sat} - 50	NaCl	0.25 - 5
Magri et al. (2005)	0 - 350	p_{sat} - 100	NaCl	
Driesner (2007)	0 - 1000	0.1 - 500	NaCl	0 - ∞
Mao and Duan (2008)	0 - 846	0.1 - 100	various	0 - 6

*Converted to SI units by Kestin et al. (1981b)

Rowe and Chou (1970) developed a function based on their own density measurements of NaCl aqueous solutions. They used three empirical coefficients for the specific volume of pure water. The deviation from pure water is represented by five additional coefficients.

Phillips et al. (1981) reviewed existing functions for various fluid properties and developed new ones for viscosity and density. The range of applicability starts at 0.25 mol_{NaCl}/kg_{H_2O} and therefore does not include pure water.

Magri et al. (2005) gave an algorithm for the calculation of the coefficients of thermal expansion and compressibility. Together with the solvent densities at a reference salinity and at solute saturation a factor is formed. Multiplying the reference density by this factor yields the solution density.

In a first study Driesner and Heinrich (2007) gave correlation formulae for phase relations in the system H_2O and NaCl. In a second study Driesner (2007) developed a set of correlations for the volumetric properties, enthalpies and heat capacities of the phases. The basic idea is that each property value at a certain temperature is equal to the property value of pure water at a different temperature. Driesner presents algorithms for the calculation of such a scaled temperature. Also a short review of various density correlations is given.

Mao and Duan (2008) developed a semi-empirical model for the density of various aqueous chloride solutions partly similar to the model by Rogers and Pitzer (1982).

2.1.2. Viscosity

Viscosity is one of the key factors in fluid flow simulation and much research has been done to measure and model brine viscosity. Table 2 lists four functions for brine viscosity calculation.

Phillips et al. (1981) modified a theoretical model proposed by Vand (1948). The ratio of solution viscosity to pure water viscosity is calculated using four coefficients.

In two publications Kestin et al. (1981a,b) developed correlations for KCl

Table 2: Applicability range of various algorithms for calculating brine viscosity.

Study	T / °C	p / MPa	Electrolytes	b / $mol \cdot kg^{-1}$
Phillips et al. (1981)	10 - 350	0.1 - 50	NaCl	0 - 5
Kestin et al. (1981b)	20 - 150	0.1 - 35	NaCl	0 - 6
Mao and Duan (2009)	0 - 350	0.1 - 100	NaCl, KCL, LiCl	0 - 6

and NaCl aqueous solutions from their own experiments. For conversion from dynamic viscosity to kinematic viscosity, the density from Rowe and Chou (1970) was used.

Mao and Duan (2009) developed a model for the viscosity of aqueous solutions of LiCl, NaCl and KCl. The algorithm uses ten parameters to calculate the ratio of solution viscosity to pure water viscosity. For calculating the viscosity of ternary mixtures, they recommend Young's mixing rule (Correia et al., 1979).

2.2. *Model of the geothermal fluid cycle*

A stationary model of a geothermal water loop has been developed. We adopted the layout of the doublet at the geothermal research site Groß Schönebeck, that consists of two connected wells, for production and injection, respectively.

Each well is equipped with several tubing segments with individual diameters and lengths. The detailed casing scheme is shown in Fig. B.13 in the appendix. The geofluid is assumed to enter or leave the well at the bottom. A downhole pump in the production well drives the hot brine through a heat extracting plant above surface, where it is cooled down from 150 °C to 60 °C. The fluid is then pumped through an injection well back into the reservoir.

The undisturbed water level in the wells is determined by the absolute pressure in the reservoir $p^{res} = 455$ bar. The absolute pressure at the production wellhead is $p_{wh}^{prod} = 15$ bar. The pressure loss in the plant is 1 bar, so the pressure at the plant outlet is $p_{wh}^{in} = 14$ bar. In order to maintain the pressure level at the production wellhead, the downhole pump has to supply a specific pressure head. In order to maintain the pressure level at the injection wellhead an injection pump or an expansion valve is assumed to be installed, depending on whether the pressure at the injection well head would be higher or lower than 14 bar without any device. The injection pump is assumed to be installed at the well head, while the expansion valve is installed downhole. The installation depth is chosen so that the pressure below the valve is ≥ 14 bar. That differs from the actual layout, where the expansion valve is installed near the surface, but it guarantees that the pressure in the model is within the validity range of the density and viscosity functions. The heat flux from the brine to the tube is neglected, and the downhole pump is assumed to work isothermally. The downhole pump works against the pressure drop due to limited productivity, injectivity of the reservoir and wall friction in the pipe. Productivity and injectivity are considered to be linear and proportional to the volumetric flow rate.

The pressure drop between the reservoir and the bottom of the production/injection well due to limited productivity/injectivity, is assumed to be a linear function of the the volumetric flow rate $\dot{V}$:

$$\Delta p_{res}^{prod} = I_P \cdot \dot{V} \tag{1}$$

$$\Delta p_{res}^{inj} = I_I \cdot \dot{V} \tag{2}$$

The factor is called productivity index I_P and injectivity index I_I, respectively. They represent the characteristics of the actual well inlet/outlet (e.g. pre-drilled liner) and the surrounding rock. So the error made by the assumption of the geofluid entering/leaving the well at the bottom is limited to the wall friction in the part of the well that is actually perforated. The wall friction is overestimated because in the model the mass flow rate is constant in the lowest part of the well, while in the case of a pre-drilled liner it is not. The contribution of viscosity to the pressure drop between well bottom and well head is, however, expected to be small compared to the difference in hydrostatic pressure. Consequently, the error is expected to be small as well.

The pressure drop Δp in a pipe segment caused by wall friction is calculated using the Prandtl-Kármán equation for the pipe friction factor λ for hydraulically smooth pipes:

$$\Delta p_{visc} = \frac{\lambda l}{d} \frac{\rho v^2}{2} \tag{3}$$

where

$$\lambda = \frac{0.309}{\log(\frac{Re}{7})} \tag{4}$$

and the Reynolds number Re is defined as

$$Re = \frac{\rho v d}{\mu} \quad . \tag{5}$$

with the pipe length l, the pipe diameter d, the brine density ρ, the brine viscosity μ. The mean flow velocity v is calculated from the volume flow rate $\dot{V}$ as follows:

$$v = \frac{\dot{V}}{\Pi \frac{d^2}{4}} \quad . \tag{6}$$

The tubing segments have been discretized in order to calculate profiles of pressure and density.

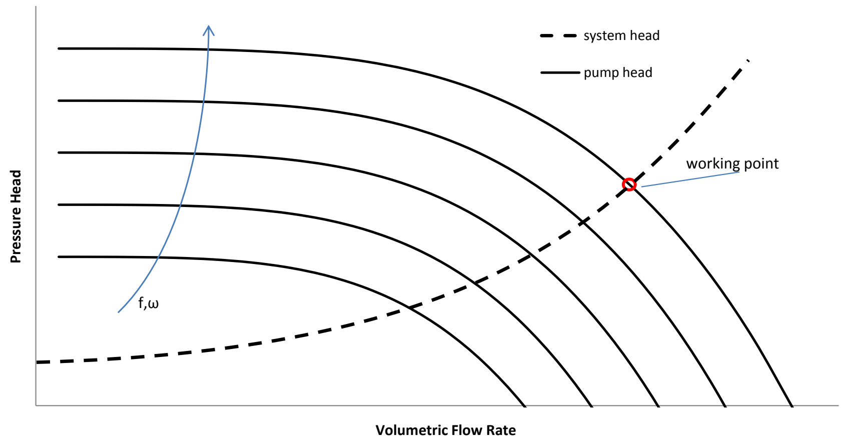

Figure 2: Schema of determination of the working point of the hydraulic system well-pump, pump characteristics (solid), well characteristics (dashed).

The pump characteristics in Fig. 2 show the relation between pressure head and volumetric flow rate for different rotational speeds. The frequency of the electric supply can be changed to control the volumetric flow of the pump and is directly proportional to its rotational speed. At a given frequency and a given pressure head the pump delivers a certain volumetric flow rate. The output power of the pump P_{out} is then calculated as:

$$P_{out} = \Delta p \cdot \dot{V} \quad . \tag{7}$$

The pump characteristics have been approximated by the following equation:

$$\Delta p \left(\dot{V} \right) = H_{max} \left(1 - \left(\frac{\dot{V}}{\dot{V}_{max}} \right)^4 \right) \tag{8}$$

where the maximum pressure head H_{max} and the maximum volumetric flow rate $\dot{V}_{max}$ are taken from the pump's technical datasheet and listed in Tab. 3.

Table 3: Maximum pump head and maximum volume for different pump frequencies (read from supplier chart).

f	H_{max}	$\dot{V}_{max}$
37 Hz	558 m	76600 l/h
42 Hz	753 m	87100 l/h
47 Hz	948 m	97600 l/h
52 Hz	1143 m	108100 l/h
57 Hz	1338 m	118600 l/h

f-pump frequency,$\dot{V}$-brine volumetric flow rate , Δp_{pump}-pump head

Fig. 2 also shows the characteristics of the well as pressure difference between between pump inlet and outlet as a function of volumetric flow rate. As mentioned above, the downhole pump has to generate this pressure difference (head) in order to maintain the pressure level at the wellhead.

The intersection between the pump and borehole characteristics, i.e. the point where the pump's volumetric flow rate and pressure head match the flow rate and the pressure drop in the pipe, represent the system's operating point.

Hence, the pressure head is calculated from the wellhead pressure p_{wh}^{prod}, the hydrostatic pressure difference above the pump Δp_{stat}^{ap}, the friction pressure loss above the pump Δp_{visc}^{ap}, the reservoir pressure p^{res}, the pressure drop between reservoir and well bottom Δp_{res}^{prod}, the hydrostatic pressure difference below the pump Δp_{stat}^{bp} and the friction pressure loss Δp_{visc}^{bp} as follows:

$$\Delta p = \left(p_{wh}^{prod} + \Delta p_{stat}^{ap} + \Delta p_{visc}^{ap}\right) - \left(p^{res} - \Delta p_{res}^{prod} - \Delta p_{stat}^{bp} - \Delta p_{visc}^{bp}\right) \quad (9)$$

where the hydrostatic pressure difference above the pump is

$$\Delta p_{stat}^{ap} = \int\limits_{pump}^{wellhead} \rho\,(p,T)\,g\,dz \tag{10}$$

and the hydrostatic pressure difference below the pump (bp) is

$$\Delta p_{stat}^{bp} = \int\limits_{wellbottom}^{pump} \rho\,(p,T)\,g\,dz\ . \tag{11}$$

Startup conditions. For a quasi-stationary simulation of the conditions at startup we assume that the brine's temperature in both wells is defined by the measured temperature profile given in Fig. 3 (Zimmermann et al., 2009). The acceleration of the brine in the pipe is neglected.

Stationary conditions. In stationary operation, we assume a constant temperature of 150 °C in the production well and a constant temperature of 60 °C in the injection well.

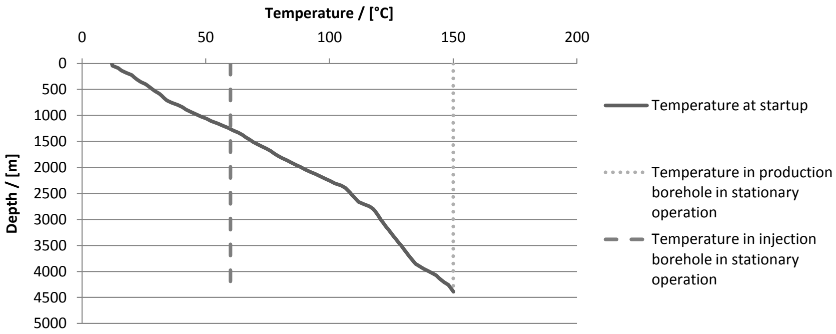

Figure 3: Temperature profiles in the boreholes for stationary and startup case.

All parameters that were used in the model are listed in Appendix B.

3. Results and discussion

3.1. Comparison of fluid property models

The different fluid density and viscosity functions presented in section 2.1 are plotted as functions of temperature, NaCl mass fraction and pressure respectively. The effect of each input parameter is discussed seperately.

Effect of temperature. With increasing temperature, both density (Fig. 4) and viscosity (Fig. 5) decrease. The maximum temperature shown is 190 °C. At the given pressure and NaCl mass fraction, the brine evaporates at about 208 °C.

The functions by Rowe and Chou (1970), Driesner (2007) and Mao and Duan (2008), in their respective range of applicability, result in almost identical densities. The function by Phillips et al. (1981) results in lower densities; the offset between Driesner (2007) and Phillips et al. (1981) lies between −1.97 % and −3.22 %. At low temperatures the function by Magri et al. (2005) results in similar values as that by Driesner (2007). For higher temperatures approximating boiling temperature, the difference increases up to −3.22 % at 190 °C.

The different functions for viscosity, in their respective application range, result in mutually consistent values. The average deviation between the functions by Phillips et al. (1981), Kestin et al. (1981b) and Mao and Duan (2009) is 0.3 % with a maximum deviation of 0.9 %.

Effect of mass fraction. With increasing NaCl mass fraction both density (Fig. 6) and viscosity (Fig. 7) increase. The maximum NaCl mass fraction

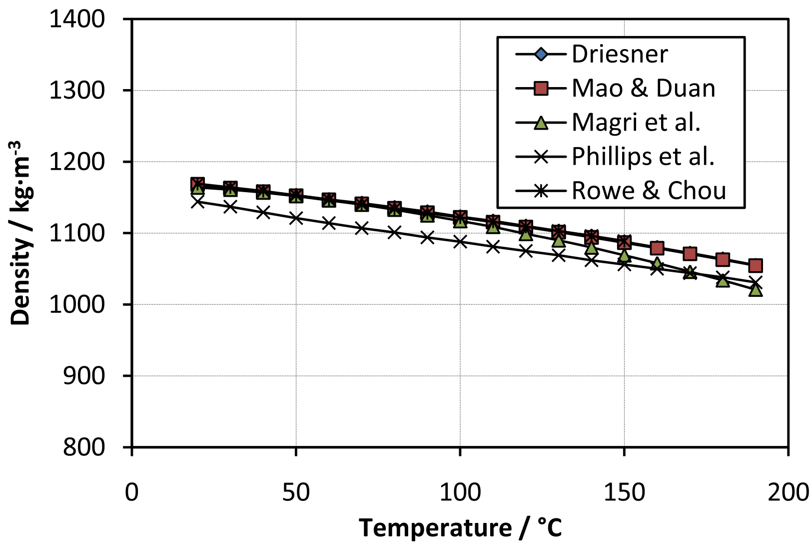

Figure 4: Density as a function of temperature at a pressure of 15 bar and a NaCl mass fraction of 0.225 $kg_{NaCl}/kg_{Solution}$.

shown is 0.275 $kg_{NaCl}/kg_{Solution}$. At the given temperature and pressure, the brine becomes oversaturated at about 0.297 $kg_{NaCl}/kg_{Solution}$.

The functions for density by Rowe and Chou (1970), Magri et al. (2005), Driesner (2007) and Mao and Duan (2008) result in accurate values for pure water. At higher NaCl mass fraction, Rowe and Chou (1970) Driesner (2007) and Mao and Duan (2008) all give values deviating less than 0.1 % from each other. The results by Magri et al. (2005) deviate increasingly with increasing NaCl mass fraction. The deviation at 0.25 $kg_{NaCl}/kg_{Solution}$ is -1.85 %. Of all functions, Phillips et al. (1981) give the lowest value for density. Compared to Driesner (2007), the values are -1.5 to -2.9 % lower.

The functions for viscosity result in consistent values, the maximum deviation is 1.4 % between Phillips et al. (1981) and Mao and Duan (2009) at

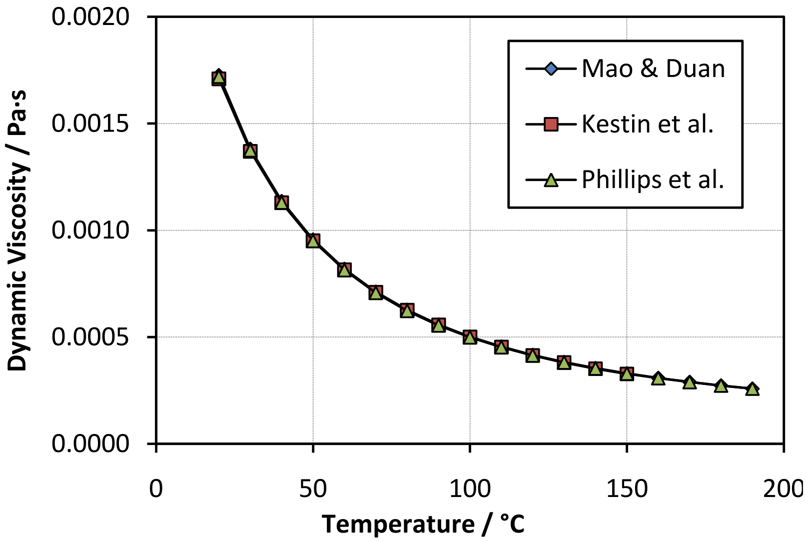

Figure 5: Viscosity as a function of temperature. The pressure and NaCl mass fraction are held constant at 15 bar and 0.225 $kg_{NaCl}/kg_{Solution}$.

a NaCl mass fraction of 0.125 $kg_{NaCl}/kg_{Solution}$.

Effect of pressure. With increasing pressure, both density (Fig. 8) and viscosity (Fig. 9) increase, but compared to temperature or NaCl mass fraction the sensitivity on pressure is low. The minimum pressure shown is 10 bar. At the given temperature and NaCl mass fraction, the brine evaporates at a pressure of about 3.9 bar.

The functions for density by Rowe and Chou (1970), Mao and Duan (2008) and Driesner (2007) result in values that deviate less than 0.2 % from each other, with the Rowe and Chou (1970) function being limited to pressures below 350 bar. The function by Magri et al. (2005) results in lower values, having a deviation of 1.8 % at 10 bar and decreasing with higher pressures.

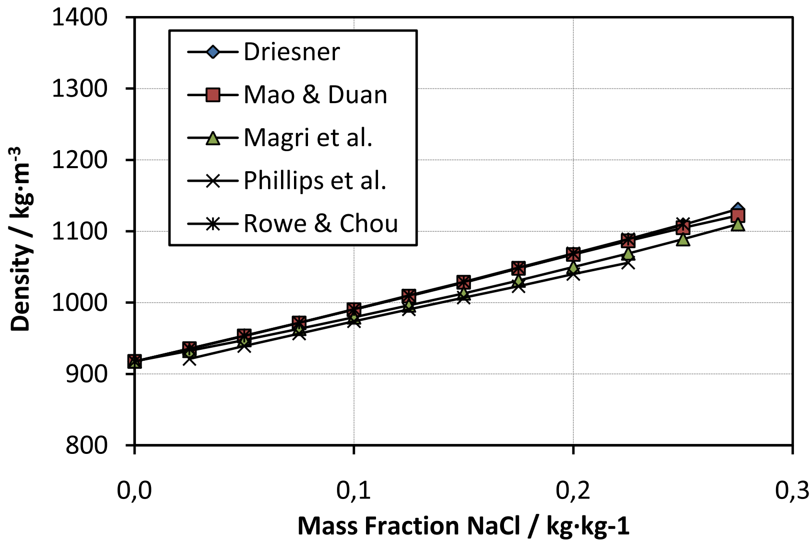

Figure 6: Density as a function of NaCl mass fraction at a temperature of 150 °C and a pressure of 15 bar.

The density calculated with the function by Phillips et al. (1981) is -2.1 to −2.7 % lower than that of Driesner (2007).

The viscosity calculated with the functions of Phillips et al. (1981) is 0.37 % lower than with those of Mao and Duan (2009) over the complete range of applicability. The values resulting from the function by Kestin et al. (1981b) are 0.8 % lower at 10 bar and 2.4 % lower at 500 bar than those of Mao and Duan (2009).

3.2. Geothermal fluid cycle

In the first step we calculated density and pressure profiles of the wells with a preset mass flow rate in order to study the deviations between values calculated with different density functions. In the second step we calculated

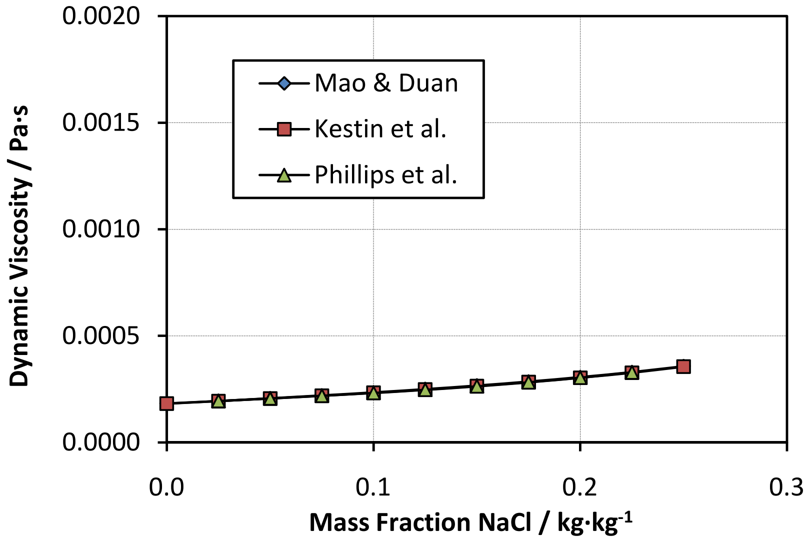

Figure 7: Viscosity as a function of NaCl mass fraction at a temperature of 150 °C and a pressure of 15 bar.

the working points of a geothermal fluid cycle in order to analyse the relevance of the differences of the property models for a geothermal application.

Density and pressure profile. The model of a geothermal fluid cycle described in section 2.2 was used to calculate density and pressure profiles for the density functions presented in section 2.1.1. The viscosity was calculated using the function by Mao and Duan (2009). That choice was made arbitrarily. The mass flow rate was set to 10 kg/s. Results are shown in Fig. 10 and 11 for density and pressure, respectively. The offsets in the profiles of the production borehole at 1100 m are caused by the production pump. The offsets in the injection borehole at 242...414 m are caused by the expansion valve described in section 2.2.

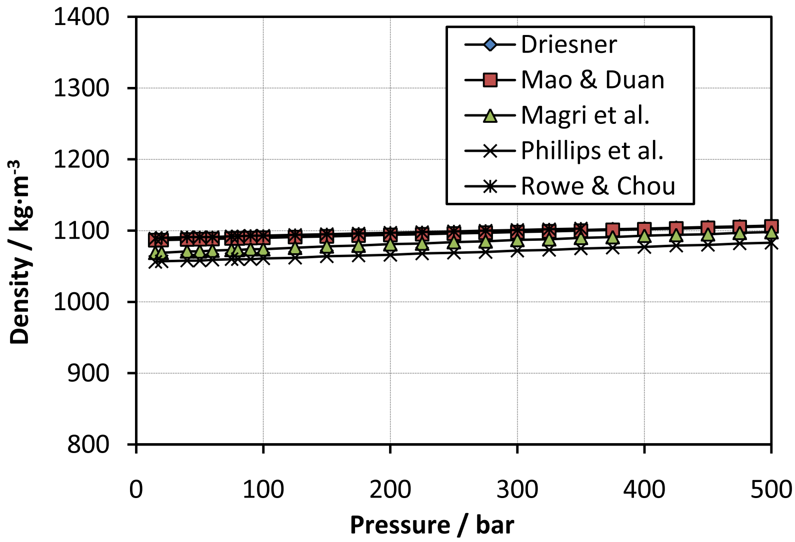

Figure 8: Density as a function of pressure at a temperature of 150 °C and a NaCl mass fraction of 0.225 $kg_{NaCl}/kg_{Solution}$.

Fig. 10 shows that, in the stationary case (constant temperature in the wells) pressure increases with depth, causing an increase in brine density. In the startup case pressure increases with depth, too, but the influence of the increase in temperature prevails so that the density decreases with depth.

In stationary operation with a brine mass flow rate of 10 kg/s at the depth of the pump inlet the pressure in the production well is 15.2 bar (average of the 4 profiles) higher than in the injection well. That means that a density difference due to temperature difference causes a pressure difference that takes load off the downhole pump.

In the production well the maximum variation of the pressure values calculated with different density functions occurs at the downhole pump inlet. At this point values deviate by up to 6.5/5.5 bar (startup/stationary)

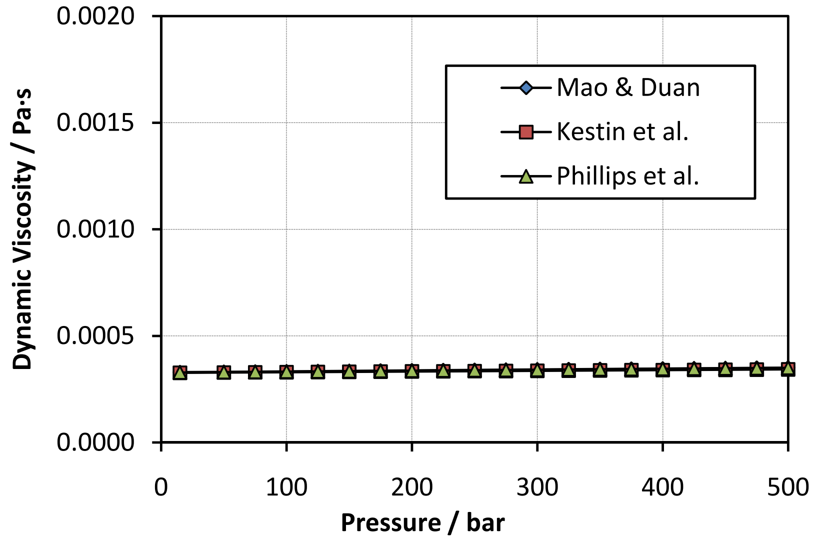

Figure 9: Viscosity as a function of pressure at a temperature of 150 °C and a NaCl mass fraction of 0.225 $kg_{NaCl}/kg_{Solution}$.

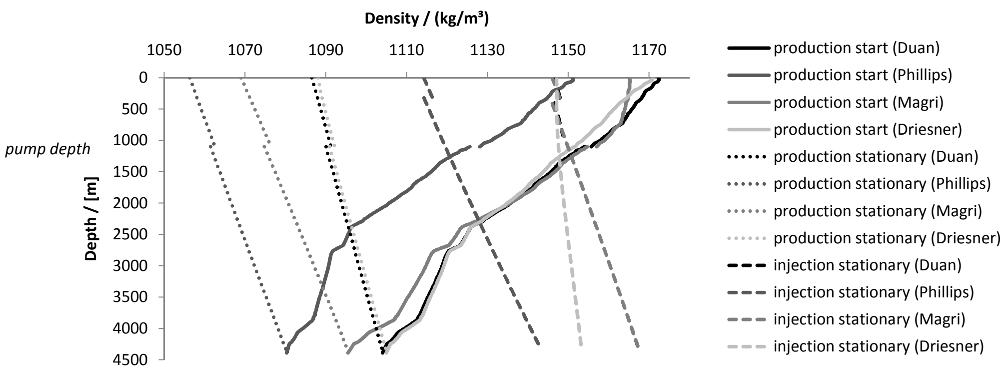

Figure 10: Density profiles of the wells for stationary case (dotted/dashed) and startup case (solid), calculated with different density correlations for a brine mass flow rate of 10 kg/s. The plots of the injection borehole at startup have been omitted for reasons of readability. Profiles are identical in both wells at startup below pump depth.

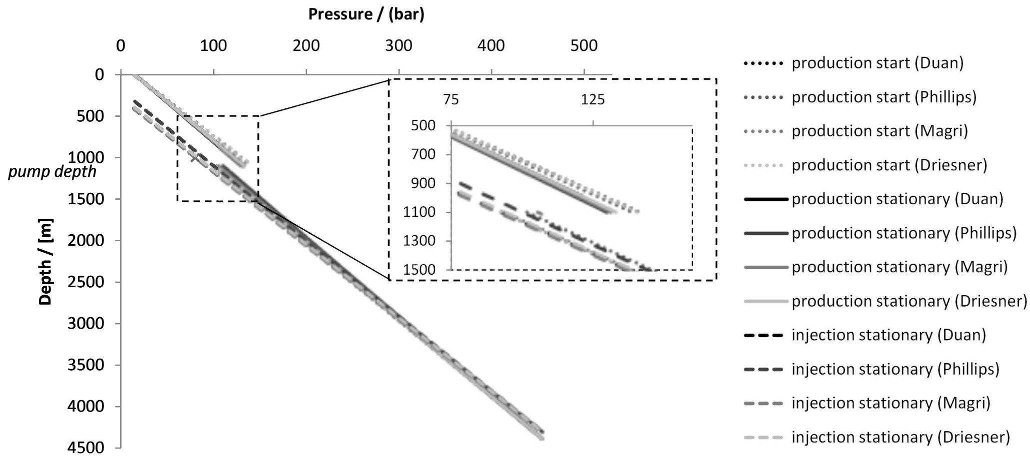

Figure 11: Pressure profiles of the wells for stationary and startup case, calculated with different density correlations for a brine mass flow rate of 10 kg/s. The plots of the injection borehole at startup have been omitted for reasons of readability. Profiles are identical in both wells at startup below pump depth.

from the average value of 95.2/104.8 bar. Putting these values in relation to the absolute pressure at the pump depth, results in a relative deviation of 6.9/5.2 %.

Deviations at the inlet and at the outlet of the pump add up to the deviation of the pressure head. We observe a maximum deviation of 8.3/7.4 bar of the pressure head from the average of 45.4/27.11 bar, being 18.4/27.5 % of the average value. A small deviation in density results in a relatively small relative deviation of the weight of the water column in the well. The absolute deviation, however, is considerably large compared to the pressure head at the pump.

Working Points. In a second step, we calculated working points at different pump frequencies (i.e. power levels) for both startup and stationary conditions. In order to do that, we applied the density functions presented in 2.1.1 except Rowe and Chou (1970) and the viscosity functions presented in section 2.1.2 to the model of the brine circuit described in section 2.2. The density function by Rowe and Chou (1970) could not be used because both pressure and temperature in the model go beyond the function's range of validity.

First, we combined one viscosity model with different density models in order to show how much the resulting working points differ from each other. Then, we combined one density model with all viscosity models to see the sensitivity on the choice of the viscosity model.

Table 4: Sensitivity on choice of density correlation. Working points of the system pump-pipe calculated for startup conditions. The viscosity function by Mao and Duan (2009) was used.

f	$\dot{V}$ / (l/s)				Δp_{pump} / bar				P_{out} / kW			
Hz	Du	P	M	Dr	Du	P	M	Dr	Du	P	M	Dr
37	4.6	8.5	4.8	4.3	59.3	56.4	58.3	59.4	25.6	43.8	25.9	23.7
42	11.4	13.8	11.6	10.6	76.3	69.7	74.8	77.4	80.7	88.4	79.4	76.4
47	16.0	17.7	16.2	15.2	88.7	80.2	86.9	91.1	131.8	130.6	128.7	128.8
52	19.7	21.1	19.8	18.9	99.0	89.4	97.0	102.8	181.2	173.3	176.6	180.6
57	23.0	24.2	23.1	22.2	108.5	98.1	106.2	113.3	231.7	218.1	225.4	233.8

Density functions: Du - Mao and Duan (2008), P - Phillips et al. (1981), M - Magri et al. (2005) and Dr - Driesner (2007)

f-pump frequency, $\dot{V}$-brine volumetric flow rate , Δp_{pump}-pump head, P_{out}-pump output power

Tables 4 and 5 show that a calculation with different density functions (cf. Fig 4) yields pressure heads at the pump that deviate by up to 7.9/7.3 % from

Table 5: Sensitivity on choice of density correlation. Working points of the system pump-pipe calculated for stationary conditions. The viscosity function by Mao and Duan (2009) was used.

f	$\dot{V}$ / (l/s)				Δp_{pump} / bar				P_{out} / kW			
Hz	Du	P	M	Dr	Du	P	M	Dr	Du	P	M	Dr
37	9.9	12.4	11.2	9.8	56.6	51.1	54.1	56.8	56.3	63.4	60.3	55.9
42	14.7	16.4	15.5	14.6	69.4	61.7	65.7	69.6	101.8	100.9	101.7	101.8
47	18.4	19.7	19.0	18.3	79.7	71.0	75.3	80.0	146.4	139.6	143.3	146.7
52	21.6	22.7	22.2	21.6	89.0	79.6	84.3	89.3	192.5	180.9	186.8	192.9
57	24.7	25.6	25.1	24.6	97.8	88.0	92.8	98.2	241.2	225.4	233.2	241.8

Density functions: Du - Mao and Duan (2008), P - Phillips et al. (1981), M - Magri et al. (2005) and Dr - Driesner (2007)

f-pump frequency, $\dot{V}$-brine volumetric flow rate , Δp_{pump}-pump head, P_{out}-pump output power

the average (startup/stationary). This causes a deviation in volumetric flow rate of up to 52/14.5 %. The strongest relative deviation of the volumetric flow rate occurs at the lowest power level. When the calculated pressure head exceeds the average, then the calculated volumetric flow rate is below the average and vice versa, due to the falling slope of the pump characteristics. That implies, that the opposite deviations of pressure head and volumetric flow rate partly cancel each other out in regard to the pump output power (cf. Eq. 7).

Tables 6 and 7 show that the influence of the choice of the viscosity model on the position of the working points is very small. This weak sensitivity is due to the fact, that viscosity has little contribution to the pressure head, compared to gravity.

Table 6: Sensitivity on choice of viscosity correlation. Working points of the system pump-pipe calculated for startup conditions. The density function by Driesner was used.

f	$\dot{V}$ / (l/s)			Δp_{pump} / bar			P_{out} / kW		
Hz	Duan	Phillips	Kestin	Duan	Phillips	Kestin	Duan	Phillips	Kestin
37	4.3	4.3	4.3	59.4	59.4	59.4	23.7	23.7	23.7
42	10.6	10.6	10.6	77.4	77.4	77.4	76.4	76.4	76.4
47	15.2	15.2	15.2	91.1	91.1	91.1	128.8	128.8	128.8
52	18.9	18.9	18.9	102.8	102.8	102.8	180.6	180.6	180.6
57	22.2	22.2	22.2	113.3	113.3	113.3	233.8	233.8	233.8

f-pump frequency, $\dot{V}$-brine volumetric flow rate , Δp_{pump}-pump head, P_{out}-pump output power

Table 7: Sensitivity on choice of viscosity correlation. Working points of the system pump-pipe calculated for stationary conditions. The density function by Driesner was used.

f	$\dot{V}$ / (l/s)			Δp_{pump} / bar			P_{out} / kW		
Hz	Duan	Phillips	Kestin	Duan	Phillips	Kestin	Duan	Phillips	Kestin
37	9.8	9.8	9.8	56.8	56.8	56.8	55.9	55.9	56.0
42	14.6	14.6	14.6	69.6	69.6	69.6	101.8	101.8	101.8
47	18.3	18.3	18.3	80.0	80.0	80.0	146.7	146.7	146.7
52	21.6	21.6	21.6	89.3	89.3	89.3	192.9	192.9	192.9
57	24.6	24.6	24.6	98.2	98.2	98.1	241.8	241.8	241.8

f-pump frequency, $\dot{V}$-brine volumetric flow rate , Δp_{pump}-pump head, P_{out}-pump output power

Differences of stationary and startup conditions. The comparison of working points calculated for startup with those calculated for stationary conditions shows the influence of the temperature profile on the volumetric flow rate. Table 8 shows that while pressure head is about 12 % higher in startup conditions, the volumetric flow rate is up to 49 % lower, resulting in a mechanic power that is up to 45 % lower.

Table 8: Sensitivity on choice of density correlation. Average values of working points and their maximum relative deviation have been calculated from Tables 4 and 5 for comparison.

f	$\dot{V}^{start}$	$\dot{V}^{stat}$	Δp^{start}_{pump}	Δp^{stat}_{pump}	P^{start}_{out}	P^{stat}_{out}
37 Hz	5.6 l/s	11.0 l/s	58.4 bar	54.5 bar	32.6 kW	59.7 kW
42 Hz	11.9 l/s	15.4 l/s	74.5 bar	66.3 bar	88.6 kW	101.9 kW
47 Hz	16.3 l/s	18.9 l/s	86.6 bar	76.1 bar	141.4 kW	144.0 kW
52 Hz	20.0 l/s	22.1 l/s	96.8 bar	85.0 bar	193.2 kW	188.0 kW
57 Hz	23.2 l/s	25.1 l/s	106.2 bar	93.6 bar	246.4 kW	234.8 kW

f-pump frequency, $\dot{V}^{start}$-brine volumetric flow rate (startup), $\dot{V}^{stat}$-brine volumetric flow rate (stationary), Δp^{start}_{pump}-pump head (startup), Δp^{stat}_{pump} - pump head (stationary), P^{start}_{out}-pump output power (startup), P^{stat}_{out}-pump output power (stationary)

As Fig. 12 and Table 8 show, the volumetric flow rate's sensitivity on pressure head is higher for low flow rates due to the flat characteristic in that region. That is why the relative difference in volumetric flow rate between startup and stationary conditions is more significant at lower pump frequencies.

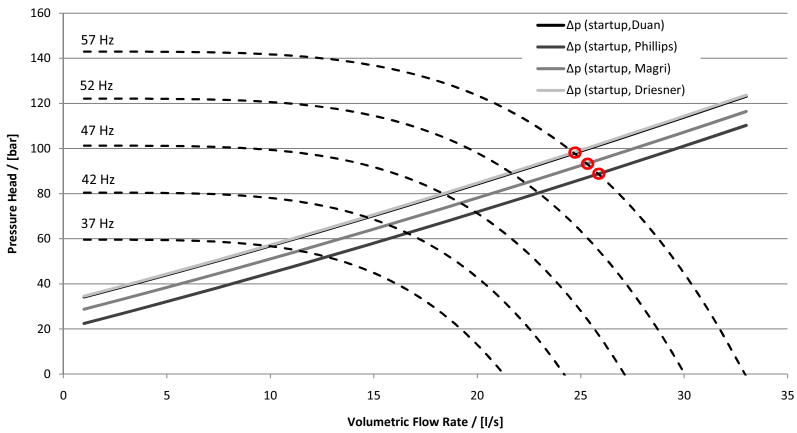

Figure 12: Characteristics of downhole pump and well, the latter calculated for four different density correlations, for startup and stationary conditions, respectively. The intersections represent working points.

4. Conclusions

We compared four density models and three viscosity models for aqueous sodium chloride solutions that are valid in the parameter range (pressure, temperature, salinity) relevant for our test site in Groß Schönebeck. The maximum deviation between calculated densities was 3 %. The agreement between calculated viscosities was very good in general, the maximum deviation was less than 2.5 %. The pressure dependency of both density and viscosity is small compared to the temperature dependency.

Although the viscosity changes by a factor of 3.5 between 150 °C and 60 °C at 15 bar and 0.225 $kg_{NaCl}/kg_{Solution}$, the influence of the choice of the viscosity function is negligible. This is due to the good agreement between different viscosity functions and the fact that viscosity related pressure drop is small compared to hydrostatic pressure differences.

As small variations in density sum up to significant variations of the pump head, the choice of density function has a strong influence on the calculated volumetric flow rate. The sensitivity of the volumetric flow rate on the pressure head of the pump is stronger at smaller flow rates, due to the pump characteristic.

Considering that an aqueous sodium chloride solution is only an approximation of natural brine and that its properties are rather well known compared to those of natural brine, the importance of choosing an adequate property function implies that the correct dimensioning of the downhole pump for a geothermal fluid cycle is a considerable challenge.

5. Outlook

Starting from here, we aim to improve several aspects of the existing model. Firstly, we intend to improve details of the model of the geothermal loop, namely the heat exchanger(s), take into account non-vertical wells, heat loss from the well to the rock and fluid inflow through a perforated liner.

Having demonstrated the importance of the fluid property model, we plan to improve two aspects of the approximation of the brine. One aspect is to take into account the real composition of the brine, which is a multicomponent fluid that contains water, NaCl, $CaCl_2$, KCl, $SrSO_4$, Fe, Mn, and dissolved gases such as N_2, CH_4, CO_2. Another aspect to be studied is the multiphase nature of the flow, including the degassing of dissolved gases and the precipitation of solids.

In order to accomplish this, we need to find a way to calculate other fluid properties, such as thermal conductivity, heat capacity, enthalpy, entropy and gas solubility. Furthermore, the chemical reactions responsible for precipitation which are triggered by changes of pressure or temperature have to to be studied in detail.

Acknowledgment

This work was performed in the framework of the GeoEn project and was funded by the Federal Ministry of Education and Reasearch of Germany.

References

Adams, J.J., Bachu, S., 2002. Equations of state for basin geofluids: algorithm review and intercomparison for brines. Geofluids 2, 257–271.

Brandt, W., 2008. Bohrtechnischer Abschlussbericht für die Bohrung Gt Groß Schönebeck 4 A(2.) (Gt GrSk 4 A(2.)) . Technical Report.

Brandt, W., 2009. Technischer Abschlussbericht für die workover Arbeiten mit coiled tubing 2009 in der Bohrung E Groß Schönebeck 3/90 . Technical Report.

Champel, B., 2006. Discrepancies in brine density databases at geothermal conditions. Geothermics 35, 600 – 606. The deep EGS (Enhanced Geothermal System) project at Soultz-sous-Forts, Alsace, France.

Correia, R.J., Kestin, J., Khalifa, H.E., 1979. Measurement and calculation of the viscosity of mixed aqueous solutions of NaCl and KCl in the temperature range 25-150 °C and the pressure range 0-30 MPa. Berichte der Bunsen-Gesellschaft für Physikalische Chemie 83, 20–24.

Driesner, T., 2007. The system H_2O-NaCl. Part II: Correlations for molar volume, enthalpy, and isobaric heat capacity from 0 to 1000 °C, 1 to 5000 bar, and 0 to 1 X_{NaCl}. Geochimica et Cosmochimica Acta 71, 4902 – 4919.

Driesner, T., Heinrich, C.A., 2007. The system H_2O-NaCl. Part I: Correlation formulae for phase relations in temperature-pressure-composition space from 0 to 1000 °C, 0 to 5000 bar, and 0 to 1 X_{NaCl}. Geochimica et Cosmochimica Acta 71, 4880 – 4901.

Hanor, J.S., 1994. Origin of saline fluids in sedimentary basins. Geological Society, London, Special Publications 78, 151–174.

Huenges, E., Winter, H., 2004. Experimente zur Produktivitätssteigerung in der Geothermie-Forschungsbohrung Groß Schönebeck 3/90. Technical Report Scientific Technical Report 04/16.

Kestin, J., Khalifa, H.E., Correia, R.J., 1981a. Tables of the dynamic and kinematic viscosity of aqueous KCl solutions in the temperature range 25–150 °C and the pressure range 0.1–35 MPa. Journal of Physical and Chemical Reference Data 10, 57–70.

Kestin, J., Khalifa, H.E., Correia, R.J., 1981b. Tables of the dynamic and kinematic viscosity of aqueous NaCl solutions in the temperature range 20–150 °C and the pressure range 0.1–35 MPa. Journal of Physical and Chemical Reference Data 10, 71–88.

Magri, F., Bayer, U., Clausnitzer, V., Jahnke, C., Diersch, H.J., Fuhrmann, J., Möller, P., Pekdeger, A., Tesmer, M., Voigt, H., 2005. Deep reaching fluid flow close to convective instability in the NE German basin–results from water chemistry and numerical modelling. Tectonophysics 397, 5 – 20. Integration of Geophysical and Geological Data and Numerical Models in Basins.

Mao, S., Duan, Z., 2008. The p,v,T,x properties of binary aqueous chloride solutions up to T=573K and 100MPa. The Journal of Chemical Thermodynamics 40, 1046 – 1063.

Mao, S., Duan, Z., 2009. The viscosity of aqueous alkali-chloride solutions up to 623K, 1,000bar, and high ionic strength. International Journal of Thermophysics 30, 1510–1523.

Phillips, S., Igbene, A., Fair, J., Ozbek, H., Tavana, M., 1981. Technical databook for geothermal energy utilization. Technical Report. LBL-12810, Lawrence Berkeley Lab., CA (USA).

Rogers, P.S.Z., Pitzer, K.S., 1982. Volumetric properties of aqueous sodium chloride solutions. Journal of Physical and Chemical Reference Data 11, 15–81.

Rowe, A.M., Chou, J.C.S., 1970. Pressure-volume-temperature-concentration relation of aqueous sodium chloride solutions. Journal of Chemical & Engineering Data 15, 61–66.

Saadat, A., Frick, S., Kranz, S., 2008. Niedertemperaturstromerzeugung - Systembetrachtung unter Berücksichtigung des Eigenbedarfs, in: Geothermische Technologien: Vom Reservoir zur Kilowattstunde ; Tagung Potsdam, 27. und 28. Februar 2008 / VDI-Gesellschaft Energietechnik, VDI. pp. 155–167.

Vand, V., 1948. Viscosity of solutions and suspensions. Part II. Experimental determination of the viscosity concentration function of spherical suspensions. The Journal of Physical and Colloid Chemistry 52, 300–314.

Zimmermann, G., Tischner, T., Legarth, B., Huenges, E., 2009. Pressure-dependent production efficiency of an enhanced geothermal system (EGS): Stimulation results and implications for hydraulic fracture treatments. Pure and Applied Geophysics 166, 1089–1106.

Appendix A. Conversion between units

For conversion between NaCl mass fraction, mole fraction and molality we used the following molar masses:

$$\mathrm{M}_{\mathrm{NaCl}} = 0.058443 \text{ kg/mol}$$

$$\mathrm{M}_{\mathrm{H_2O}} = 0.018015 \text{ kg/mol}$$

NaCl mass fraction w_{NaCl}.

$$[w_{\mathrm{NaCl}}] = \frac{\mathrm{kg}_{\mathrm{NaCl}}}{\mathrm{kg}_{\mathrm{Solution}}} \tag{A.1}$$

$$w_{\mathrm{NaCl}} = \frac{b \cdot \mathrm{M}_{\mathrm{NaCl}}}{(1 + b \cdot \mathrm{M}_{\mathrm{NaCl}})} \tag{A.2}$$

NaCl mole fraction x_{NaCl}.

$$[x_{\mathrm{NaCl}}] = \frac{\mathrm{mol}_{\mathrm{NaCl}}}{\mathrm{mol}_{\mathrm{Solution}}} \tag{A.3}$$

$$x_{\mathrm{NaCl}} = \frac{b \cdot \mathrm{M}_{\mathrm{H_2O}}}{(1 + b \cdot \mathrm{M}_{\mathrm{H_2O}})} \tag{A.4}$$

Molality b.

$$[b] = \frac{\mathrm{mol}_{\mathrm{NaCl}}}{\mathrm{kg}_{\mathrm{H_2O}}} \tag{A.5}$$

$$b = \frac{w_{\mathrm{NaCl}}}{(1 - w_{\mathrm{NaCl}})\mathrm{M}_{\mathrm{NaCl}}} \tag{A.6}$$

$$b = \frac{x_{\mathrm{NaCl}}}{(1 - x_{\mathrm{NaCl}})\mathrm{M}_{\mathrm{H_2O}}} \tag{A.7}$$

Appendix B. Model parameters

Table B.9: Parameters used in brine circuit calculations

plant (above ground facility)	
pressure drop in heat exchanger	1 bar
brine pressure inlet	15 bar
brine	
brine temperature at extraction	150 °C
brine temperature at injection	60 °C
salt concentration	225 g/kg
pump	Centrilift 45-HC10000
pump frequency	37...57 Hz
position (depth)	1100 m
reservoir	
productivity index	15 m^3/hMPa
injectivity index	15 m^3/hMPa
pressure	455 bar

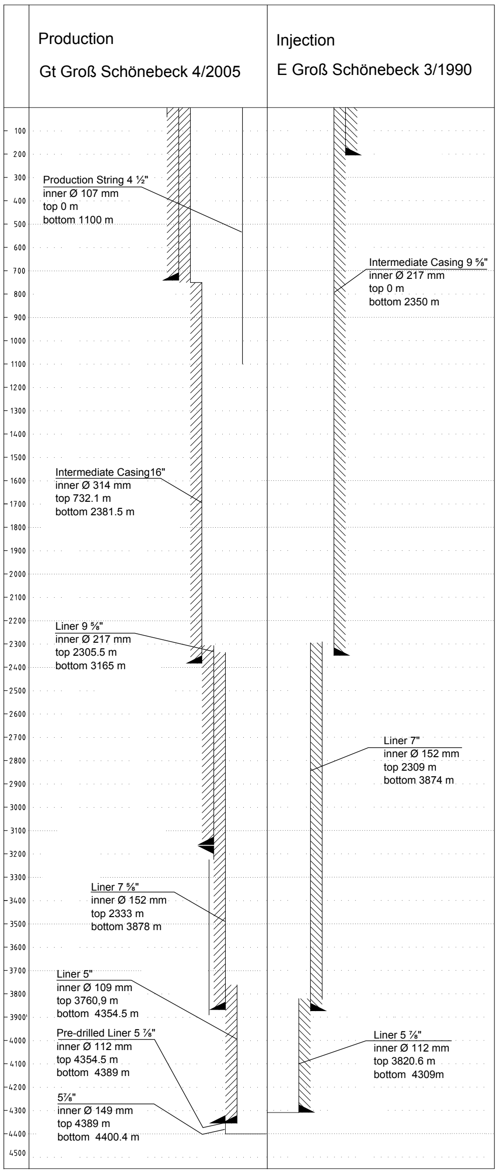

Figure B.13: Casing scheme for the production borehole Groß Schönebeck 4/2005 and the reinjection borehole Groß Schönebeck 3/1990, adapted from Brandt (2009, 2008).